

Anticorrosive Self-Assembled Hybrid Alkylsilane Coatings for Resorbable Magnesium Metal Devices

Avinash J. Patil,^{†,□,○} Olivia Jackson,[†] Laura B. Fulton,[†] Dandan Hong,^{†,□,○} Palak A. Desai,[‡] Stephen A. Kelleher,[§] Da-Tren Chou,[†] Susheng Tan,^{||,⊥} Prashant N. Kumta,^{†,‡,□,○,△,▼} and Elia Beniash^{*,†,‡,□,○}

[†]Department of Bioengineering, Swanson School of Engineering, University of Pittsburgh, 302 Benedum Hall, 3700 O'Hara Street, Pittsburgh, Pennsylvania 15261, United States

[‡]Department of Biological Sciences, Dietrich School of Arts and Sciences, University of Pittsburgh, 4249 Fifth Avenue, Pittsburgh, Pennsylvania 15260, United States

[§]Department of Biology, Oberlin College, Science Center K123, 119 Woodland Street, Oberlin, Ohio 44074, United States

^{||}Department of Electrical and Computer Engineering, Swanson School of Engineering, University of Pittsburgh, 1238 Benedum Hall, 3700 O'Hara Street, Pittsburgh, Pennsylvania 15261, United States

[⊥]Petersen Institute for NanoScience and Engineering (PINSE), University of Pittsburgh, Benedum Hall, 3700 O'Hara Street, Pittsburgh, Pennsylvania 15261, United States

[#]Department of Oral Biology, School of Dental Medicine, University of Pittsburgh, 347 Salk Hall, 3501 Terrace Street, Pittsburgh, Pennsylvania 15261, United States

[□]Center for Craniofacial Regeneration, University of Pittsburgh, 501 Salk Pavilion, 335 Sutherland Drive, Pittsburgh, Pennsylvania 15261, United States

[○]McGowan Institute for Regenerative Medicine, University of Pittsburgh, 450 Technology Drive, Suite 300, Pittsburgh, Pennsylvania 15219, United States

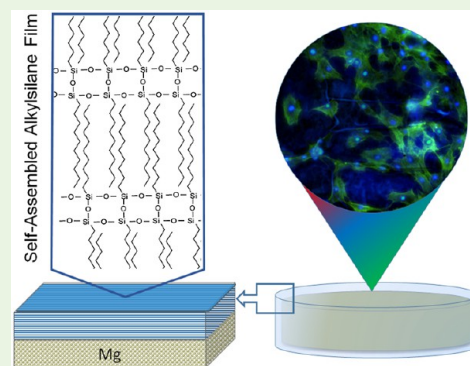
[△]Department of Chemical and Petroleum Engineering, University of Pittsburgh, 940 Benedum Hall, 3700 O'Hara Street, Pittsburgh, Pennsylvania 15261, United States

[▼]Department of Mechanical Engineering and Materials Science, University of Pittsburgh, 636 Benedum Hall, 3700 O'Hara Street, Pittsburgh, Pennsylvania 15261, United States

Supporting Information

ABSTRACT: Magnesium (Mg) and its alloys are promising candidates for use as resorbable materials for biomedical devices that can degrade in situ following healing of the defect, eliminating the need for a second surgery to remove the device. Hydrogen gas is the main product of magnesium corrosion, and one of the limitations for use of Mg devices in clinic is the formation of gas pockets around them. One potential solution to this problem is reducing the rate of corrosion to the levels at which H₂ can diffuse through the body fluids. The study's aim was to evaluate the potential of hybrid alkylsilane self-assembled multilayer coatings to reduce Mg corrosion and to modify physicochemical properties of the coatings using surface functionalization. The coating was made by copolymerization of n-Decyltriethoxysilane and Tetramethoxysilane followed by dip coating of metal discs. This resulted in a formation of homogeneous, micron thick, and defect free coating. The coated surface was more hydrophobic than bare Mg, however functionalization of the coating with 3-aminopropyltriethoxysilane reduced the hydrophobicity of the coating. The coatings reduced several fold the rate of Mg corrosion based on the H₂ evolution and other assessment methods, and effectively prevented the initial corrosion burst over the first 24 h. In vitro tissue culture studies demonstrated cytocompatibility of the coatings. These results reveal excellent anticorrosive properties and good cytocompatibility of the hybrid alkylsilane coatings and suggest great potential for use of these coatings on resorbable Mg devices.

KEYWORDS: magnesium, AZ31, resorbable, implant, alkylsilane, coating, corrosion, self-assembly, cytocompatibility



1. INTRODUCTION

Magnesium is a great candidate for use in resorbable devices because of its lightweight, mechanical properties closely matching

Received: September 25, 2016

Accepted: February 24, 2017

Published: February 24, 2017

natural bone, low toxicity, and high corrosion characteristics.^{1,2} Moreover, Mg²⁺ can activate osteogenic differentiation and promote bone formation.^{3–6} Attempts to use Mg as a biomaterial trace back to the 19th century when several physicians and surgeons were experimenting with Mg for orthopedic, cardiovascular and other applications.⁷ However, these initial attempts faced limitations because the corrosion reaction of Mg produces H₂, leading to formation of gas pockets around the device and increases the pH thus significantly limiting the applicability of Mg in the biomedical field.⁷ Furthermore, fast, uncontrolled degradation can also lead to premature resorption of the devices. In the last couple of decades, a renewed interest in biomedical use of Mg has developed, with researchers around the world trying to overcome these obstacles. There are two major approaches for control of Mg degradation rate, namely developing new alloys with desirable corrosion properties^{8,9} and use of anticorrosive coatings.¹⁰ In addition to corrosion regulation, coatings can be used as controlled release systems,^{11,12} and surface modifications of the coatings with bioactive molecules can improve tissue regeneration around coated devices.^{13,14} A number of different chemistries are used for anticorrosive coatings, including organic polymers,^{15,16} inorganic minerals,^{17,18} peptides,¹⁹ and polysiloxanes.^{20–23}

Use of aliphatic alkylsilanes (AS) provides means to introduce structural organization into the coating through self-assembly, allowing for greater control of the coating properties and increased functionality of the coatings.^{24–27} ASs, and specifically alkyltriethoxysilanes (C_nTES) with general formula C_nH_{2n+1}(SiOEt)₃ can form self-assembled multilayered films on solid surfaces. C_nTES molecules become amphiphilic upon hydrolysis and self-assemble into multilayered films comprising 3–4 nm thick lamellae, with alkyl tails of these amphiphilic molecules forming hydrophobic cores and silane heads undergo polycondensation, leading to formation of cross-linked polysiloxane planes sandwiching the hydrophobic cores.^{24–26} The properties of the film can be modified by changing the length of the alkyl tails, by adding UV cross-linkable moieties²⁵ or by copolymerizing with other siloxanes, such as tetraethoxysilane (TEOS) or tetramethoxysilane (TMOS).²⁴ Furthermore, surface functionalization of these films can be achieved using well developed chemistries.^{28,29} Another advantage of these coatings is that they comprise biocompatible and biodegradable compounds such as hydrocarbons (fat) and polysiloxanes, which are widely used as biomaterials.^{30–33}

The aim of this study was to design anticorrosive hybrid self-assembled AS coatings for implantable Mg devices. We assessed compositional, structural and anticorrosive properties of the coatings, conducted surface functionalization of the coatings and tested cytocompatibility of the coatings in vitro in tissue culture.

2. MATERIALS AND METHODS

All the reagents were purchased from Sigma-Aldrich (St. Louis, MO, USA) and used as received unless otherwise stated.

2.1. Metal Sample Preparation. Six mm diameter discs were stamped from 1 mm thick Mg (99.9% purity) and AZ31 alloy (96% Mg, 3% Al, and 1% Zn) sheets (Alfa Aesar, Ward Hill, MA, USA) and polished with 1200 grit (5 μm) MicroCut SiC abrasive discs (Buehler Inc., Lake Bluff, IL, USA). The polished discs were then etched in etching solution comprising 20 mL of 85% Glycerol, 5 mL of 65% HNO₃, and 5 mL of glacial acetic acid for 60 s. Chemical etching was done to remove debris, impurities and the oxide layer from the surface of the metal and to smooth the scratches introduced during polishing. Etched discs were sonicated in acetone for 30 min and stored under vacuum until further use. Prior to the alkylsilane coating, a thin uniform

hydroxide layer was formed on the discs by immersion in 3.0 M sodium hydroxide (NaOH) solution for 2 h. In addition to the passivating properties, MgOH₂ provides means for covalent binding of the silanes to the metal surface as described elsewhere.^{21,34,35}

2.2. Synthesis and Deposition of Self-Assembled Multilayer AS Coating on Mg and Mg Alloys. Self-assembled hybrid AS films on Mg and AZ31 alloys were prepared by a dip-coating technique as described elsewhere.^{24–26} The precursor solution was prepared by mixing 0.25 mL (0.73 mM) of n-decyltriethoxysilane (DTEOS) (Alfa Aesar, Ward Hill, MA, USA), 0.43 mL (2.92 mM) of tetramethoxysilane (TMOS) (Alfa Aesar, Ward Hill, MA, USA), 2 mL (0.032 mM) of ethanol, and 0.25 mL of 0.010 M HCl (aq). The precursor solution was stirred for 24 h at room temperature to induce hydrolysis of DTEOS and TMOS. Mg or AZ31 alloy discs passivated with NaOH were dip-coated in the solution for 1 min and dried in air for 10 min at room temperature. The discs were subsequently dried in an incubator at 37 °C for 24 h for removal of any trace amount of organic solvents.

2.3. Functionalization of the Coatings. For functionalization with 99% pure 3-aminopropyltriethoxysilane (APTES), the following solution was prepared: 0.25 mL of 0.01 M HCl was added to a mixture of 2.0 mL of ethanol (EtOH) and 0.43 mL of APTES solution. This precursor solution was stirred for 24 h at room temperature prior to functionalization. The AS-coated samples were then dipped in the APTES solution at room temperature for 1 min and dried in air for 10 min at room temperature. The disc was subsequently dried in an incubator at 37 °C for 24 h for removal of any trace amount of organic solvents.

Four groups of samples were used in this study as follows:

- Polished and etched Mg and AZ31 discs (Mg, AZ31)
- NaOH treated Mg and AZ31 discs (Mg–OH; AZ31–OH),
- AS coated NaOH treated Mg and AZ31 discs (Mg–OH–AS; AZ31–OH–AS)
- APTES functionalized AS coated Mg and AZ31 discs (Mg–OH–AS–APTES; AZ31–OH–AS–APTES).

2.4. Scanning Electron Microscope (SEM) Characterization.

The surface morphology of the uncoated and AS coated Mg and AZ31 discs were studied using JSM-6330F (JEOL, Peabody, MA, USA) SEM at 3.0–20.0 kV operating voltage and the working distance of 10 mm. All samples were sputter-coated with gold prior to SEM using Cressington sputter coater 108 auto model (Cressington Scientific Instruments Ltd., Watford, United Kingdom). The elemental composition of the noncoated and coated samples were analyzed using energy-dispersive X-ray spectroscopy (EDS) in SEM. EDS INCA analysis system (Oxford Instruments, Oxfordshire, UK) equipped with a beryllium-window protected Si (Li) detector was used for the elemental analysis at the operating voltage of 15 kV.

To assess the thickness of the coating, we created a several micrometer deep trough in some samples using the focused ion beam milling (FIB). The ion milling and imaging was done on a FEI SCIOS Focused Ion Beam/Scanning Electron Microscope dual beam system with gallium ion source (Thermo Fisher Scientific, Waltham, MA, USA). Au/Pt depositions were carried out before the ion milling to protect the coating from the gallium ion beam.

2.5. Atomic Force Microscopy (AFM) Characterization. High-resolution AFM was used to assess the thickness of individual lamellae by scanning the surface of AS coatings deposited on AS coated Mg films deposited on glass substrates (generous gift from Dr. Sergey Yarmolenko, NCAT, Greensboro, NC). Use of Mg films instead of polished disks significantly reduced the roughness of the samples, allowing high-resolution AFM imaging of the samples. The AFM analysis was carried out using a Veeco Dimension V scanning probe microscope (SPM) controlled by a Nanoscope V controller (Bruker Corporation, Billerica, MA, USA). Tapping mode was employed with an AFM probe of 58–80 kHz nominal resonance frequency and ~3 N/m spring constant. The acquired images were flattened using the Nanoscope V software. Measurements were carried out on the flattened images.

2.6. Attenuated Total Reflectance Fourier Transform Infrared (ATR-FTIR) Spectroscopy Characterization. The AS coatings on the Mg and AZ31 substrates were analyzed by Vertex-70 ATR-FTIR (Bruker Optik GmbH, Ettlingen, Germany) using a diamond Miracle ATR accessory (Pike Technology, WI, USA). Spectra were obtained at 4 cm^{-1} resolution averaging 120 scan in the $400\text{--}4000\text{ cm}^{-1}$ frequency range.

2.7. Contact Angle Measurement. The wettability of the AS coated Mg and AZ31 discs were assessed by the sessile drop ($5\ \mu\text{L}$, Milli-Q water) contact angle measurement using VCA 2000 Goniometer (AST Products, Billerica, MA, USA).

2.8. In Vitro Corrosion Analyses. The corrosion resistance of AS coated Mg and AZ31 discs was measured using hydrogen evolution method, weight loss assessment, and electrochemical corrosion tests.

Hydrogen Evolution Test. The H_2 evolution was measured in a simulated body fluid (SBF) pH 7.2, prepared according to a published formulation by Kokubo³⁶ (Table S1), at room temperature over 24 h and a 7 day period. Each sample group was prepared in triplicate and the samples were immersed in SBF. A glass graduated measuring cylinder was placed over the samples in a glass beaker to collect the released gases (Figure S1). The experiments were carried out for 1 week and the solution was changed on day 2, 4, and 6. The ratio of solution volume to the total surface area of the tested samples was kept above 6.7 to mimic in vivo degradation behavior of Mg.^{19,37,38} The SBF level in each beaker was maintained constant throughout the study to avoid evaporation effects affecting the validity of the measurements.

Weight Loss Analysis. The mass loss analysis after 7 days of degradation in SBF at room temperature was performed according to ASTM G1 standards and works by Lorking³⁹ and Bobe et al.⁴⁰ Prior to corrosion experiments all the samples were weighted using a microbalance Mettler Toledo XPE26 (Mettler Toledo, Columbus, OH, USA). After experiments, the corroded sample discs were removed from SBF and placed in a beaker containing an aqueous solution of CrO_3 at a concentration of $\sim 180.0\text{ g/L}$. The beaker was sonicated for 10 min to remove the corroded products in the chromic acid solution. The chromic acid solution was changed between samples to ensure complete removal of the corroded products. After chromic acid cleaning, the sample discs were rinsed with deionized water followed by absolute ethanol. The sample discs were completely dried in a vacuum desiccator overnight and weighed. The percentage weight change was calculated for all the samples.

Electrochemical Corrosion Test. Electrochemical measurements of the noncoated Mg and AS-coated Mg and AZ31 alloy samples were performed using a CH604A electrochemical workstation (CH Instruments Inc., Austin, TX, USA). All the samples were prepared as described above (sections 2.1 and 2.2); one side of each sample disc was connected to an electric wire with conductive silver-containing epoxy and then electrically insulated with an epoxy resin, such that a working area of 0.283 cm^2 was exposed to the electrolyte for electrochemical testing. A platinum wire was used as the counter electrode and an Ag/AgCl electrode (4.0 M KCl, Accumet, Fisher Scientific, MA, USA) as the reference electrode. Electrochemical measurements were carried out in a three neck water circulated jacket flask (Ace Glassware, NJ, USA) filled with 120 mL of SBF and maintained at room temperature. Each sample was immersed in the SBF and then the stable open circuit potential (OCP) was monitored for 10 min, before starting the potentiostatic polarization test at a scan rate of 1.0 mV s^{-1} . The CHI 604A software program was used to perform the analysis and plot the data. The corrosion current density (I_{corr}) and corrosion potential (E_{corr}) were determined by the Tafel extrapolation method.^{41,42}

2.9. Cell Culture Experiments and Cytocompatibility Tests. Tissue Culture Experiments on AS-Coated Mg Discs. MC3T3 cells were seeded on Mg-OH-AS and Mg-OH-AS-APTES discs ($n = 3$ per group) with the seeding density of $10,000\text{ cells cm}^{-2}$ and cultured for 15 days in phenol red free α -MEM medium (Catalog number: 41061-029, Thermo Fisher Scientific, MA, USA) supplemented with 10% FBS and 1% penicillin/streptomycin at $37\text{ }^\circ\text{C}$ and 5% CO_2 . The medium was changed every 3 days. After 15 days, cells were stained with Hoechst 33342 NucBlue Live Ready Probes nuclear stain (Thermo-Fisher Scientific, Waltham, MA, USA) and ActinGreen 488 ReadyProbes

f-actin stain (Life Technologies, Carlsbad, CA, USA) following the manufacturer's protocols. After three washes in PBS, samples were studied using a Nikon TE2000 microscope (Nikon Instruments Inc., Melville, NY, USA) in epifluorescence mode using a DAPI filter for nuclear DNA staining and FITC filter for F-actin staining. Micrographs were captured and processed using Nikon NIS Elements software.

Cell density on Mg-OH-AS, Mg-OH-AS-APTES discs after 15 days in tissue culture was calculated from integrated DAPI fluorescence intensity in 3 epifluorescence micrographs per group. Each micrograph contained $53.49 \times 10^4\ \mu\text{m}^2$ ($731.42\ \mu\text{m} \times 731.42\ \mu\text{m}$) field of view. A blue channel was isolated from RGB images using ImageJ image processing package (ImageJ, Bethesda, MD). The grayscale of each image was adjusted to minimize the background intensity. In each micrograph 10 nuclei were randomly selected and their integrated intensity values were measured. The average signal intensity per nucleus was calculated for each image, and the integrated intensities of the images were divided by corresponding average nucleus intensities, providing us with the total cell number per image. Cell density on the discs was presented as a number of nuclei per $1 \times 10^4\ \mu\text{m}^2$.

Tissue Culture Experiments on AS-Coated Glass Coverslips. In a separate set of experiments, MC3T3 cells were seeded on bare glass coverslips (CS), AS coated coverslips (CS-AS) and AS-coated coverslips functionalized with APTES (CS-AS-APTES). The cells were seeded at a density of $10,000\text{ cells cm}^{-2}$ and allowed to grow for 2 weeks in phenol red free α -MEM supplemented with 10% FBS and 1% penicillin/streptomycin at $37\text{ }^\circ\text{C}$ and 5% CO_2 .

The cells were counted using the method described in the previous section. In addition, the number of cells was calculated using a spectrophotometric method. The amount of DNA per coverslip was assessed on the 7th and 14th day in culture by spectrophotometric assay using NanoDrop 1000 (Thermo-Fisher Scientific, Waltham, MA, USA) in each experimental group in triplicates. The number of cells per coverslip was calculated using a conversion factor of $7.6\text{ pg of DNA per cell}$.⁴³ Cell density was calculated as a number of nuclei per $1 \times 10^4\ \mu\text{m}^2$.

AlamarBlue fluorescence assay (Thermo-Fisher Scientific, Waltham, MA, USA) was used to monitor cell viability.⁴⁴ AlamarBlue assays were conducted at first, third, seventh and 14th day in triplicates according to the manufacturer's protocol. In brief, the culture medium was replaced with 1 mL 10% v/v alamarBlue reagent in complete growth medium and the samples were incubated for 4 h at $37\text{ }^\circ\text{C}$. After the incubation, the alamarBlue solution was collected and replaced with regular medium and the tissue culture samples were allowed to grow until the next time point. This design allowed us to monitor the metabolic activity in individual samples over a 2-week period. Fluorescence intensity of each sample was calculated as an average of 3 separate readings measured at excitation/emission wavelengths of 530/590 nm using a Synergy H1 microplate reader (BioTek instruments, Winooski, VT, USA). The wells containing only alamarBlue solution in medium were used as controls for background fluorescence correction.

The cells grown for 1, 3, 5, and 7 days on all three experimental substrates were studied using SEM. The samples were washed twice with phosphate buffered saline (PBS), fixed in 2.5% glutaraldehyde in 0.1 M PBS (pH 7.4) for 10 min and washed thoroughly with 0.1 M PBS for $3 \times 15\text{ min}$. The samples were further fixed in 1% OsO_4 in 0.1 M PBS for 60 min and washed thoroughly with 0.1 M PBS for $3 \times 15\text{ min}$. Each sample was dehydrated in a graded ethanol series (concentrations 30%, 70% and 100%) for $3 \times 15\text{ min}$. After dehydration, samples were immersed in Hexamethyldisilazane (HMDS) solution for 15 min and subsequently air-dried overnight and sputter coated with gold prior to SEM using Cressington sputter coater 108 Auto (Cressington Scientific Instruments Ltd., Watford, UK). The SEM analysis was conducted using JSM-6330F (JEOL, Peabody, MA, USA) at $3.0\text{--}20.0\text{ kV}$ operating voltage and the working distance of 10 mm.

2.10. Statistical Analysis. All the experiments were performed in triplicate for each experimental group and time point. The data were compared between groups using analysis of variance (ANOVA) followed by Tukey's multiple comparison test with 95% confidence level in Origin Pro 2015 software (OriginLabs, Northhampton, MA USA). The data were presented as mean \pm standard deviation (S.D.).

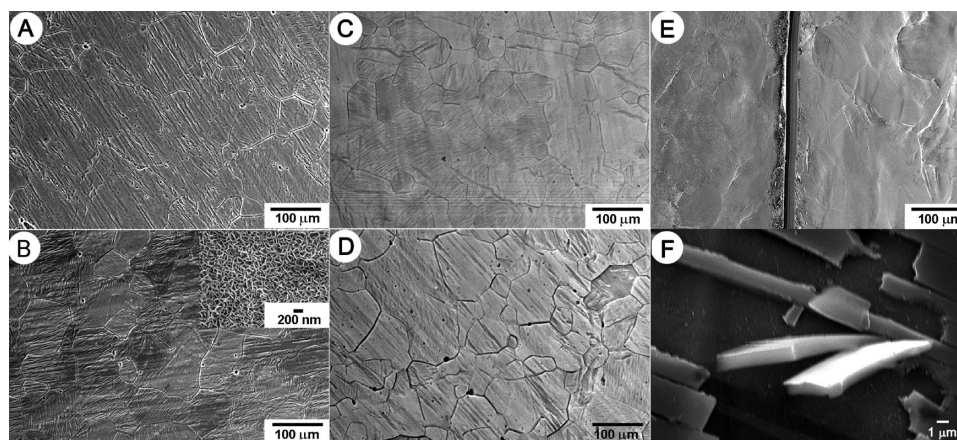


Figure 1. SEM micrographs of (A) uncoated Mg, (B) Mg-OH, Inset shows a high-magnification micrograph of a Mg-OH surface, (C) Mg-OH-AS; (D) Mg-OH-AS-APTES; (E) low-magnification Mg-OH-AS scratched surface; and (F) a higher-magnification image of a Mg-OH-AS scratched surface with pieces of AS coating peeling off the surface.

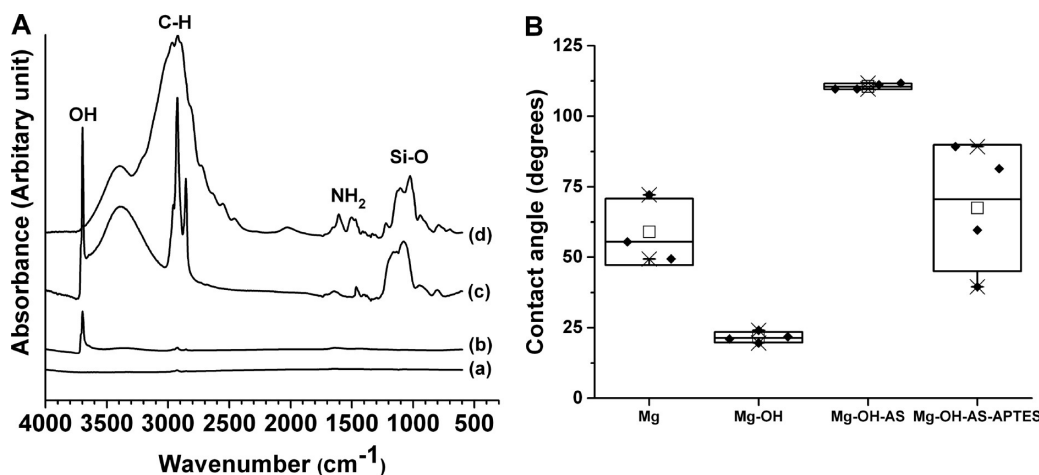


Figure 2. (A) ATR-FTIR spectra of (a) Mg, (b) Mg-OH, (c) Mg-OH-AS, (d) Mg-OH-AS-APTES and (B) box graph of static water contact angles measured on Mg sample discs.

3. RESULTS

3.1. SEM Characterization. SEM characterization of the coatings was conducted to assess the structural integrity of the AS films (Figure 1). Analysis of the polished and etched Mg surface revealed individual grains, grain boundary contours and the shallow scratch marks produced by polishing (Figure 1A). At the intermediate magnification, the alkali treated surface appeared very similar to the bare Mg surface (Figure 1B). However, a nanostructured hydroxide layer on the Mg surface was clearly recognizable at a higher magnification (Figure 1B'). Dip-coating procedure produces a micron thick uniform AS film on the Mg-OH disc (Figure 1C). Interestingly, because the AS films are extremely thin, the grain boundaries of the underlying metal were clearly visible. APTES functionalized AS coated discs had similar appearance to AS coated discs (Figure 1D). The grain boundaries and scratch marks were still visible on this sample although they were less pronounced, suggesting that the coating followed the surface topography. Scratching of the AS coated samples with a scalpel did not lead to major defects of the coating away from the scratched mark (Figure 1E). Analysis of the broken coating in the scratched area allowed us to determine the thickness of the AS coating by measuring the pieces of the coating detached from the metal surface (Figure 1F). On the basis of this analysis, the thickness was approximately 1 μm .

To further assess the coating thickness, we created a several micrometer deep trough in the coated samples using FIB. The analysis of the sample cross-sections showed that the coating is $\sim 1 \mu\text{m}$ thick (Figure S2).

3.2. AFM Analysis. To assess the thickness of individual AS lamellae comprising the coating, we have conducted the AFM study of the AS coated Mg films. Edges of multiple lamellae are exposed on the surface creating step like patterns (Figure S3). By measuring the height of these steps an average thickness of the lamellae was determined to be 2.8 nm (SD = 0.6; $n = 9$) which is in a good agreement with the lamellae thickness data reported elsewhere.^{24,26}

3.3. ATR-FTIR Analysis. ATR-FTIR spectroscopy was used to analyze the chemical composition of the coatings on the Mg surface. Figure 2A shows the spectra of noncoated and AS coated Mg discs. Polished and etched Mg discs did not show any major absorbance peaks, as expected (Figure 2A), whereas alkali-treated discs presented a sharp peak around 3600 cm^{-1} consistent with the -O-H stretching band. The spectra of Mg-OH-AS coating reveal peaks in the 1045–1127 cm^{-1} that correspond to Si-O asymmetric stretching in -Si-O-Si- bond (Figure 2A). The C-H stretching in the alkyl chain of DTEOS is evident around 3000–2850 cm^{-1} . After amination with APTES, the -NH₂ absorption band appeared in the 1500–1700 cm^{-1} region, indicating the

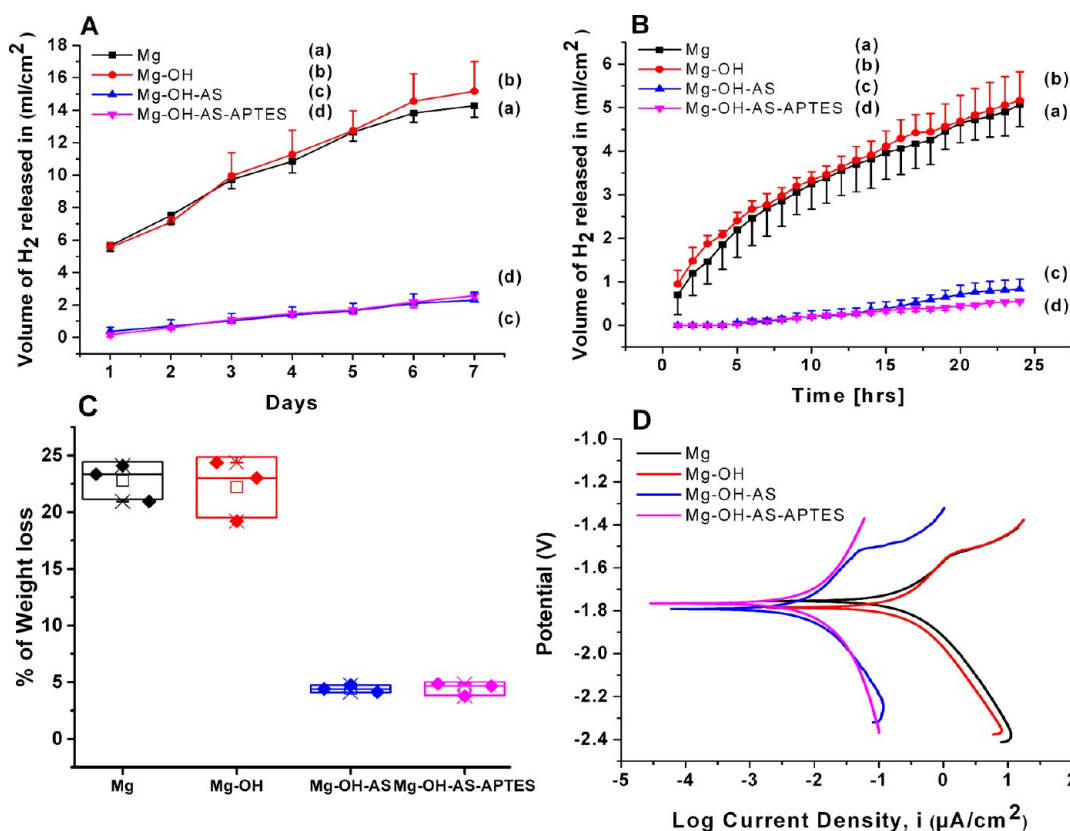


Figure 3. Cumulative hydrogen release profiles from Mg discs incubated in SBF over (A) a 7 day period, (B) 24 h period; (C) weight loss of Mg discs incubated in SBF for 7 days; and (D) potentiodynamic polarization curves of Mg sample discs.

presence of amines on the surface of the coating. Results of the experiments with AZ31 samples were similar (Figure S4A).

3.4. Contact Angle Measurement. The surface wettabilities of noncoated Mg, alkali-treated Mg, and AS-coated Mg were examined by measuring the static contact angle using deionized water droplet. The contact angle of polished and etched Mg discs was approximately $58.98 \pm 11.78^\circ$ (Figure 2B). Alkali treatment of Mg surface made it more hydrophilic and significantly reduced the contact angle down to $21.62 \pm 1.87^\circ$ ($p \leq 0.05$). The static contact angle of AS coated samples was $110.60 \pm 1.05^\circ$, indicating the hydrophobic nature of these samples. The contact angle of these samples was significantly higher than both Mg ($p \leq 0.01$) and Mg-OH samples ($p \leq 0.0001$). Amination of the AS layer with APTES significantly reduced the contact angle of the surface to $67.44 \pm 22.43^\circ$ ($p \leq 0.01$), and made it similar to the bare Mg discs ($P > 0.05$). The results of contact angle analysis on AZ31 samples showed similar trends (Figure S4B).

3.5. Determination of the Corrosion Rate by H₂ Evolution and Weight Loss Methods. Cumulative H₂ released from the uncoated Mg discs over 7 days was ~7 fold higher than that of AS-coated Mg discs; this difference was highly significant ($p < 0.0001$) (Figure 3A). The alkali treatment did not have any significant effect on the extent of corrosion over the 7 days period. The hydrogen release profiles of the Mg-OH-AS and Mg-OH-AS-APTES groups were not significantly different ($p > 0.9974$) (Figure 3A, Table S2). Experiments with AZ31 samples yielded similar results (Figure S5A, Table S2).

To assess the ability of the AS coating to slow down the initial burst of corrosion, we have followed H₂ evolution over the initial 24 h after immersion of the discs in SBF. The results of these

experiments indicate that the AS coating reduced the initial Mg corrosion rate 5 fold from 0.16 to 0.03 mL/h, effectively preventing the initial burst of corrosion (Figure 3B, Table S2).

After the initial 24 h, the corrosion rate of noncoated samples significantly decreased and achieved steady state (Figure 3B, Table S2). This decrease in the corrosion rate can be potentially attributed to deposition of corrosion products, which can have a passivating effect. Nevertheless, the corrosion rate of the AS coated Mg over the following 6 day period was 4.5 times lower than that of the bare Mg, 0.013 mL/h vs 0.06 mL/h, (Figure 3A, Table S2). The results of the experiments with AZ31 were very similar to those obtained with Mg (Figure S5B, and Table S2).

The results of the weight loss measurements were in excellent agreement with the hydrogen release experiments. Both Mg and Mg-OH samples showed significantly higher % weight loss compared to Mg-OH-AS and Mg-OH-AS-APTES samples (Figure 3C). The weight loss of the Mg-OH was similar to Mg group. Weight loss measurements of AZ31 samples also yielded similar results (Figure S5C).

3.6. Determination of the Corrosion Rate by Potentiodynamic Polarization and Impedance Spectroscopy Technique. The average corrosion potential (E_{corr}) measured for the untreated Mg discs was -1.77 V and it was not significantly different from Mg-OH ($p = 0.81$), Mg-OH-AS ($p = 0.93$) and Mg-OH-AS-APTES ($p = 0.55$) samples (Figure 3D, Table 1). A slightly more negative value of E_{corr} was observed for both Mg and AZ31 coated samples suggesting a weak dependence of the thermodynamic corrosion potential on the coating system and the nature of the coated films. However, the potentiodynamic polarization curves for the coated Mg samples were shifted to lower I_{corr} values compared to pure Mg indicative

of the changes in corrosion kinetics. Passivation of the Mg discs with alkali did not seem to show a significant change ($p < 0.75$) in the I_{corr} value compared to the noncoated Mg discs, likely due to the porous nature of the hydroxide layer. The AS coated Mg discs, however, showed a significant reduction in the I_{corr} value compared to noncoated Mg discs ($p < 0.0002$) (Figure 3D, Table 1). Moreover, APTES functionalized AS

Table 1. Corrosion Potential (E_{corr}) and Current Density (I_{corr}) Values for Noncoated and Coated Mg and AZ31 Substrate

treatment	E_{corr} (V) (SD)	I_{corr} ($\mu\text{A}/\text{cm}^2$) (SD)
Mg bare	-1.77 (0.014)	171.97 (26.40)
Mg-OH	-1.75 (0.027)	151.84 (31.78)
Mg-OH-AS	-1.78 (0.020)	10.85 (3.93)
Mg-OH-AS-APTES	-1.80 (0.038)	3.66 (2.56)
AZ31 bare	-1.49 (0.009)	96.43 (65.90)
AZ31-OH	-1.54 (0.032)	100.84 (50.26)
AZ31-OH-AS	-1.62 (0.014)	6.06 (1.13)
AZ31-OH-AS-APES	-1.59 (0.006)	4.07 (3.04)

coated Mg discs showed an almost 50 times reduction in I_{corr} values compared to the noncoated Mg discs ($p < 0.0001$). We observed similar trends in the electrochemical corrosion parameters for the AZ31 samples (Figure S5D, Table 1).

3.7. SEM Analysis of the Sample Surfaces after Incubation in SBF. SEM and light microscopy observations of the discs incubated in SBF for 7 days reveal that the AS coating lead to a significant decrease in formation of corrosion products, in agreement with our hydrogen evolution and weight loss assessments (Figure 4). The SEM micrographs of the uncoated

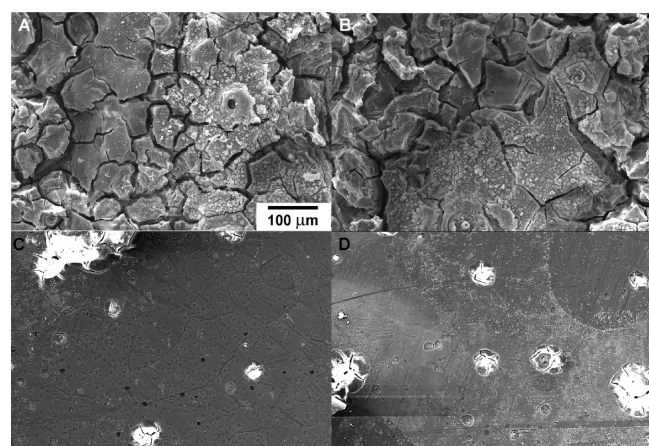


Figure 4. SEM images showing the surface morphologies of (A) uncoated Mg, (B) Mg-OH, (C) Mg-OH-AS, (D) Mg-OH-AS-APTES after 1-week incubation in SBF. All micrographs are taken at the same magnification.

samples show the presence of surface cracks and corrosion products on the untreated and alkali treated Mg discs (Figure 4A, B). The SEM analysis of the coated Mg discs revealed a much better surface preservation. The surface of both Mg-OH-AS and Mg-OH-AS-APTES samples were for the most part intact with a few areas, 200 μm or less across, in which the surface of the coating was pushed out by the expanding corrosion products, leading to cracking of the coating (Figure 4C, D). This observation suggests that initial stages of pitting corrosion are occurring under the coating.

3.8. Cytocompatibility Studies. Tissue Culture Experiments on AS-Coated Mg Discs. Tissue culture experiments were conducted to assess the cytocompatibility of the AS coated Mg discs. MC3T3 cells were seeded on Mg discs coated with AS (Mg-OH-AS) and aminated AS (Mg-OH-AS-APTES) and the tissue culture experiments were carried out for 2 weeks in α -MEM medium. After 15 days in culture, the cells were present on both nonaminated and aminated AS coated discs. Light microscopy revealed that the cells formed a dense confluent layer with a well-developed actin cytoskeleton (Figure 5), suggesting

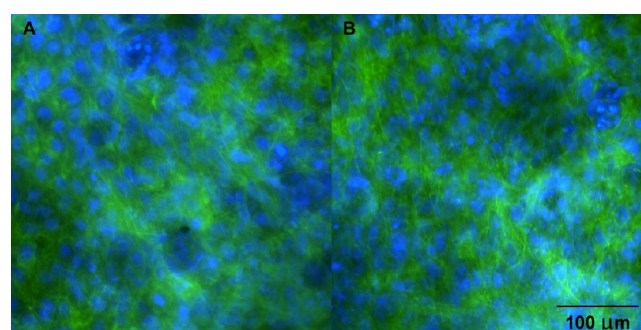


Figure 5. Epifluorescence images of MC3T3 cells grown for 15 days on (A) Mg-OH-AS and (B) Mg-OH-AS-APTES coated Mg discs. The actin cytoskeleton is visualized using Alexa Fluor 488 dye (green) and nuclear DNA is stained with Hoechst 33342 dye (blue).

that the coated discs are cytocompatible and sustain cell adhesion and proliferation. The cell density was not significantly different on AS-coated vs AS-coated aminated discs (13 cells/ $100 \mu\text{m}^2$ vs 15 cells/ $100 \mu\text{m}^2$, $p = 0.38$, Figure 6A), which indicates that hydrophobicity of the coating does not have a long lasting effect on cell proliferation.

Tissue Culture Experiments on AS-Coated Glass Coverslip. Tissue culture studies on the Mg discs pose some limitations, such as the lack of transparency, which restricts light microscopy observations, as well as the porosity and chemical composition of the corrosion products which interfere with many biological assays.⁴⁵ To further assess the cytocompatibility of the AS films themselves we conducted a series of experiments using MC3T3 cells plated on bare glass coverslips, AS coated glass coverslips and AS coated and aminated glass coverslips. During the experiments cell morphology was monitored by light microscopy and SEM. Cell density was calculated from fluorescent images as described in the preceding section and using spectrophotometric DNA assay. Cell vitality was assessed using alamarBlue metabolic assay.

We conducted cell density analysis in a manner used for the quantification of cells on the coated Mg discs from the fluorescence images of tissue cultures on the samples from all 3 experimental groups at day 7 and 14 (Figure 6B). No significant differences were observed between the experimental groups at each time point while significant differences in cell densities were observed in each experimental group between day 7 and day 14. We also compared the cell density on the AS coated and AS-coated and aminated glass coverslips with similarly treated Mg disks 2 weeks in the cell culture. The statistical analysis revealed that the cell density on the AS coated and aminated Mg samples was significantly higher than the cell density on the coated glass coverslips ($p = 0.03$ for Mg-OH-AS-APTES vs CS-AS and $p = 0.001$ for Mg-OH-AS-APTES vs CS-AS-APTES). No significant difference was observed between the Mg-OH-AS

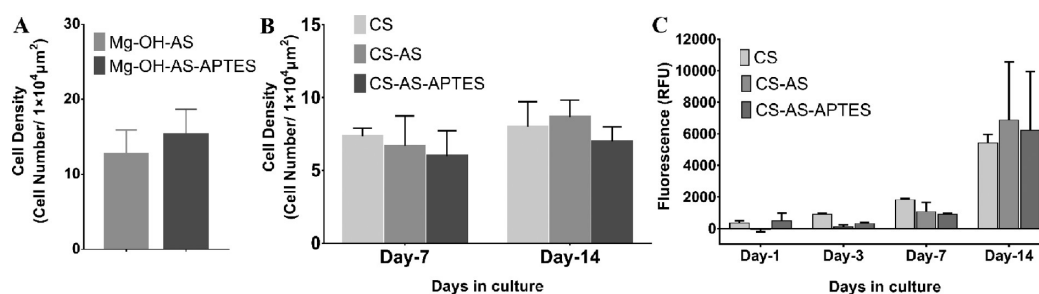


Figure 6. (A) Cell density on AS coated Mg discs after 15 days in culture. (B) Changes in cell density on glass coverslips and glass coverslips coated with AS over 2-week period. (C) Cell viability, determined by alamarBlue assay, on glass coverslips and glass coverslips coated with AS films.

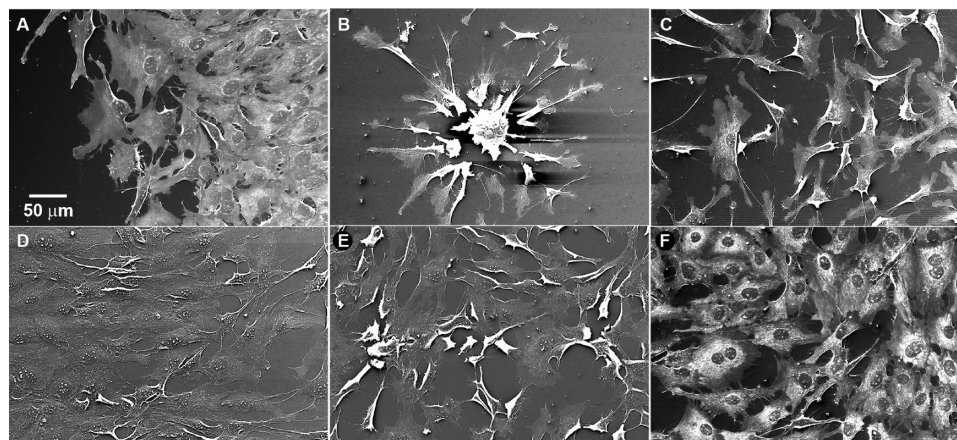


Figure 7. SEM images showing cells morphologies on uncoated and AS-coated glass coverslips. (A, D) Cells on uncoated glass coverslips 24 h and 5 days after seeding. (B, E) Cells on AS-coated glass coverslips 24 h and 5 days after seeding. (C, F) Cells on AS-coated and aminated glass coverslips 24 h and 5 days after seeding. All micrographs were taken at the same magnification.

group and both coated glass coverslip groups. Overall, our results demonstrate that the AS coatings can sustain cell proliferation over a 2-week period in the tissue culture conditions at a rate similar to or higher than on the glass coverslips. We also conducted spectrophotometric assays of the cells grown on non-coated, AS coated and AS coated and aminated glass coverslips. These studies did not reveal any statistically significant differences in the cell density at each time point (Figure S6). At the same time, the cell density on day 14 was significantly higher than on day 7 in all 3 experimental groups ($p = 0.002$). These results indicate that AS coatings support cell proliferation in the tissue culture conditions.

AlamarBlue incubations were conducted at day 1, 3, 7, and 14. At each time point, the fluorescence intensity values were not statistically different among the groups, suggesting that there were no differences in cell viability on different substrates. At the same time, for all 3 groups the changes in the fluorescence intensity over time were highly significant ($p < 0.0001$), potentially reflecting increases in cell density. Overall, the results of these studies demonstrate that the viability and the metabolic activity of the cells grown on the AS films is similar to the cells grown on glass coverslips, indicating that the AS coatings are cytocompatible. Light microscopy and SEM studies revealed that 1 day after plating the cells on the bare glass coverslips and on the AS-coated and aminated glass coverslips were well attached and spread on the surface of the substrate (Figure 7A, C; Figure S7). In contrast, cells on the AS-coated substrates formed aggregates, potentially in an attempt to minimize their interactions with a hydrophobic substrate (Figure 7B, Figure S7). By day 3, this clustering has significantly diminished and by day 5 the cell layer

was indistinguishable from the cell layers formed on the bare coverslips (Figure 7D–F, Figure S7). We also conducted studies of the acting cytoskeleton on the AS coated and bare glass coverslips which showed no observable differences between the groups (Figure S8).

3.9. Elemental Composition of the Coated Mg Surfaces after 2 Weeks in the Tissue Culture. The coated Mg samples were studied with SEM after exposure for 15 days to the cell culture conditions. The coatings were present on the surfaces although multiple cracks have formed leading to the typical mud crack appearance of the surface (Figure 8A). Minimal amounts of the corrosion products and debris were present on the disc surfaces, however most of the surface area was clear. EDS analysis of the surfaces has revealed strong O and Si K edge signals from the surface of the coating consistent with the presence of siloxanes in the coatings, while Mg signal was consistently confined to the crevices of the cracked regions (Figure 8B–E). Interestingly, only traces of Ca and no P were detected by EDS (Table 2), potentially due to the restricted access of Ca^{2+} and PO_4^{-3} to the metal surface and lower surface pH of the coating. This is remarkable because calcium phosphate is typically present on the corroding Mg surfaces exposed to body fluids^{46–48} (Figure S9 and Table S3).

4. DISCUSSION

The results of our study show that AS coating produces micrometer-thick, smooth and homogeneous films with excellent anticorrosion properties. Importantly, these coatings can not only slow down the corrosion rate but effectively prevent the initial burst of corrosion over the first 24 h of the exposure. Hence,

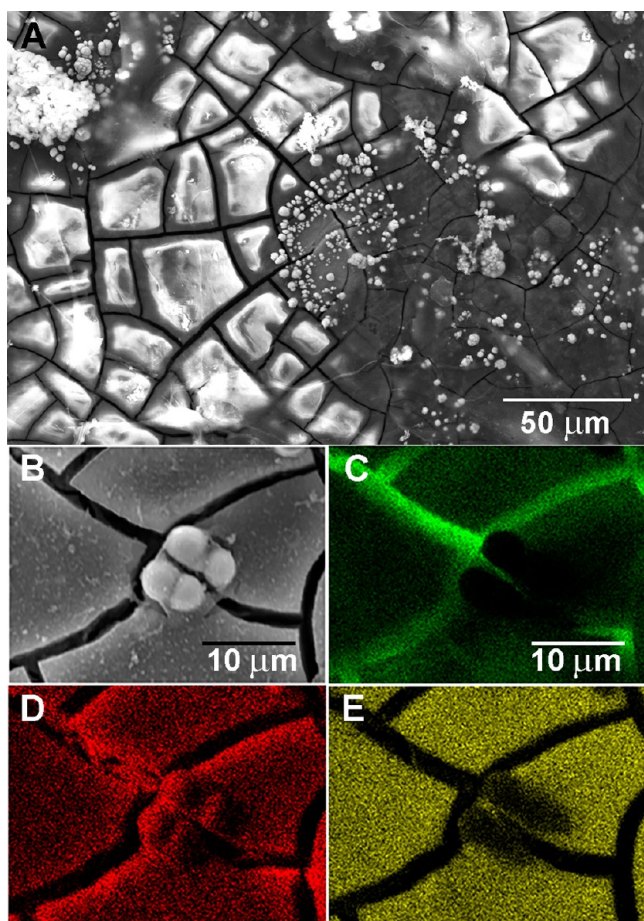


Figure 8. Surface of Mg-OH-AS sample exposed for 2 weeks to tissue culture conditions. (A) SEM micrograph of the surface; (B) SEM micrograph of an area of the surface used for the EDS mapping; (C) Mg map of the area in B, (D) O map of the area in B; (E) Si map of the area in B.

Table 2. Elemental Analysis Using Energy Dispersive X-ray Spectroscopy (EDS) of the Surface of Mg-OH-AS Discs Exposed for 15 Days to the Tissue Culture Conditions

element K edge	wt %	at %
O K	36.46	48.39
Mg K	33.58	29.32
Si K	28.15	21.28
Cl K	0.77	0.46
Ca K	1.05	0.55

these coatings can potentially reduce the formation of gas pockets around Mg implantable devices, which is one of the limitations for use of Mg in medical applications.⁷ Our data also indicate that AS coatings can reduce spontaneous precipitation of calcium phosphates on the device surfaces. Our *in vitro* tissue culture data demonstrate good cytocompatibility of the AS coatings. Overall, the results of our studies demonstrate a high potential of AS films for use in coating applications for degradable Mg devices. Smooth surface morphology and homogeneity of AS coatings are important factors in the reduction of corrosion.^{49–51} Furthermore, the lamellar nanostructure of the AS films with alternating hydrophobic alkyl and covalently bound polysiloxane layers can provide an effective barrier for the solution access to the implant surface. We have assessed anticorrosive properties of the AS coatings by three independent methods commonly used in the corrosion research,

namely, hydrogen evolution,^{37,52,53} weight loss,^{39,54,55} and potentiodynamic polarization.^{56–58} The results obtained by the three independent methods agreed extremely well and demonstrated a dramatic decrease in the corrosion rate. In agreement with the corrosion studies, our SEM observations of the coated samples revealed that AS layer remained relatively intact after 7 days in SBF and 14 days in cell culture medium. Importantly, the results of H₂ release analysis over the first 24 h clearly demonstrate that AS coating effectively prevents the initial hydrogen release burst, which is critical for preventing or minimizing gas pocket formation at the most critical time—immediately after surgery. A number of earlier studies showed that the corrosion rate is fastest during the first day after immersion of Mg in aqueous solution, leading to a corrosion burst and fast formation of gas pockets around the device.^{2,6,9,59,60} After the initial burst, the rate of corrosion typically slows down and enters a steady-state phase. The slowdown of the corrosion can be mainly attributed to a combination of two factors, namely an increase in the pH and formation of Mg hydroxide and Mg/Ca phosphate layer on the metal surface.⁶⁰ We have noticed in our experiments an increase in pH from 7.2 to 8.2 over a 7 day period. Therefore, it is possible that a pH increase can affect the corrosion rate. At the same time, the fact that the SBF changes did not lead to any significant changes in the corrosion rate indicates that the accumulation of the corrosion products on the metal surface is the primary factor affecting the rate of corrosion.

A number of coating strategies were used over the years to control corrosion of Mg and its alloys including Ca phosphate,^{61,62} Mg fluoride,¹⁸ polymer,^{16,63} and others coatings.¹⁰ Gray-Munro et al.⁶² used calcium phosphate coating on AZ31 alloy discs. They demonstrated that calcium phosphate coating did not have a significant effect on the overall corrosion rate of AZ31 alloy. Synthetic and natural polymers were also used to control the corrosion rate of Mg and its alloys. Park et al.⁶⁴ used a dip coating technique to form polycaprolactone (PCL) coating on Mg samples. Our results suggest that AS coating has better anticorrosive properties compared to PCL. Specifically, 3.8 mL/cm² H₂ released from Mg discs coated with PCL by single dipping in 1 day. Even after 10 iterations of dip-coating by PCL, only a small decrease in corrosion was observed. In contrast, a single step dip-coating with AS substantially reduces the corrosion rate (2.3 mL/cm² H₂ released over 7-days period). Gray-Munro et al.⁶² used poly(L-lactic acid) (PLA) coating on AZ31 discs and observed that PLA coating led to a significant reduction of corrosion vs bare AZ31 sample. Our results demonstrated that AS coating of AZ31 samples led to a significantly greater reduction of the corrosion rate compared to PLA coating, with the corrosion rate of AS coated samples at 0.2815 mg/day vs 5.6 mg/day of the PLA coatings. Cui et al.¹⁹ used a biomimetic peptide comprising three Asp-Ser-Ser (DSS) amino acid repeats based on the highly acidic dentin matrix protein, phosphophoryn. The average daily H₂ evolution rate of the peptide-coated AZ31 was 0.96 mL/cm² compared to 0.35 mL/cm² with the AS-coated AZ31. The higher corrosion rate in the case of DSS₃ peptide-coated AZ31 is likely due to the poor coverage of the peptide coating and its high hydrophilicity. In contrast the AS coating minimizes the solution access to the metal surface due to its homogeneity and its lamellar structure comprising alternating hydrophobic alkyl and poly siloxane layers.²⁵ Although it is often difficult to compare results of studies using different experimental design, overall, our analysis of the literature indicates that the micrometer-thick AS coatings

provide corrosion control that is better or comparable to other deposited coating systems.

It has been reported that a hydroxide conversion layer on Mg surface can slow down initial corrosion.^{10,39,65,66} We saw a small but significant decrease in corrosion in Mg–OH samples by weight loss and H₂ evolution methods. Interestingly, potentiodynamic polarization experiments did not show any significant differences between Mg and Mg–OH in both E_{corr} and I_{corr} . Potentially, this can be due to the high variability of the bare Mg and Mg–OH data. Also, the hydroxide layers formed by the alkali treatment typically result in porous coatings which do not have a strong bearing in differentiating the surface from the pristine metal. Hence, despite the presence of hydroxyl species, the porous surface does not alter the E_{corr} as well as the I_{corr} values. In addition to passivation of the Mg surface, alkali treatment might further improve adhesion of the coating layer to Mg surface because of its higher surface area and the presence of hydroxyls that provide a substrate for covalent bonding of silanes.²⁹

Because of the hydrophobic nature of the AS-coated layers, there is a reduction in SBF diffusion and electron transport toward the Mg surface, resulting in decrease in the total cathodic current density.²¹ The hydrophobic AS layer acts as a physical barrier preventing access of the aqueous medium to the metal surface. Further modification of the coating with APTES did not reduce the I_{corr} value significantly, which is expected because the surface functionalization did not change the structural and chemical properties of the bulk of the AS layer. The mud cracked appearance of the coating after prolonged exposure to the cell culture medium potentially suggests that after initial breach of the coating layer in blister-like point defects, the corrosion propagates along the grain boundaries and the forming corrosion products push against the coating layer, leading to the crack generation. The fact that, unlike many polymer coatings, the AS layer does not delaminate from the surface, supports the notion that it is tethered to the surface via covalent bonds with the hydroxide layer, as shown elsewhere.^{21,34,35}

One critical requirement for the biomedical coatings is low toxicity and good biocompatibility. Results of our in vitro tissue culture studies demonstrate that AS coatings support cell proliferation and active cell metabolism at the same rate as the uncoated glass coverslips in 2-week long experiments. Furthermore, the results of our tissue culture experiments demonstrate that MC3T3 cells can survive, spread, proliferate, and maintain high cell density on the surface of AS-coated Mg samples for 2 weeks.

Good adsorption of biomolecules and cell attachment are beneficial for the integration of orthopedic implantable devices,⁶⁷ while reducing cell and protein attachment might be important for cardiovascular applications.⁶⁸ It is therefore essential that the coating exhibits surface chemistry characteristics optimal for a specific application. Among the various surface characteristics, surface wettability profoundly affects the protein adsorption and cell attachment to the surface.^{69,70} In the case of polymers, optimal wettability for cell attachment was observed on the moderately hydrophilic surfaces.⁶⁹ In our experiments, we did not see any differences in cell attachment between hydrophobic and hydrophilic coatings a few days after seeding; however, in the first day after seeding, cells form aggregates in an attempt to minimize their interactions with hydrophobic AS coatings. It is possible that a layer of biomolecules is formed on the hydrophobic surface with time, allowing for cell spreading.

In the earlier in vitro studies, cells directly seeded on the coated Mg samples were followed only for several days.^{16,45,68,71}

Typically, cells cannot survive on the corroding Mg surfaces more than 48 h and other coatings reported in the literature would degrade much faster than the AS hybrid self-assembled coatings. The fact that the cells could survive and proliferate on the AS coated Mg samples is quite remarkable. The only long-term study we were able to identify was the study by Kunjukunju et al.⁶³ in which the cells were cultured on AZ31 coated with MgF₂ and poly-L-lysine/chitin multilayer over 2 weeks. In this study the cell density after 14 days was similar to the one on Ti. At the same time it is hard to compare these results with ours, since the alloy corrosion was extremely low in these experiments and the seeding density was much higher. There were several tissue culture in vitro studies of the cytocompatibility of the silanated substrates. The study by Curran et al.⁷² has shown that the number of cells on the aminated surfaces after 7 days was significantly higher than on methylated or bare glass surfaces. In another study (3-Glycidioxypropyl)trimethoxysilane coated Ti samples were tested in vitro for 14 days in the primary gingival fibroblast tissue culture.⁷³ The cell density on the coated surfaces was 1.4×10^5 , close to the cell density in our experiments and 40% higher than in the Ti group.⁷³ Overall, the AS coatings demonstrate cytocompatibility that is similar or better than other siloxane-based coatings.

5. CONCLUSIONS

In this study, we used a dip-coating technique to self-assemble alkylsilane multilayer films on degradable Mg and AZ31 alloy to control their corrosion rate. We further functionalized the alkylsilane layer with APTES to reduce its hydrophobicity and improve cell adhesion. We finally tested cytocompatibility of the coated Mg samples in vitro under tissue culture conditions. Our results clearly demonstrate that AS coatings can effectively reduce the corrosion rate and prevent the initial burst of corrosion, which in situ can lead to the formation of gas pockets around an implantable device. We further demonstrate that the AS coatings can be functionalized to modify physicochemical properties, i.e., wettability, or bioactivity of the device. In our in vitro tissue culture experiments, cells survived and proliferated on the AS-coated Mg discs for more than 2 weeks, which indicates that the coatings are not cytotoxic and support cell attachment, spreading, and proliferation. Importantly, no calcium or phosphate was detected on the sample surface after 2 weeks under tissue culture conditions, suggesting that the coating can prevent calcium phosphate formation. Overall, our study clearly demonstrates a great potential for the use of hybrid AS coatings for the corrosion control and biocompatibility of the resorbable Mg devices.

■ ASSOCIATED CONTENT

Supporting Information

The Supporting Information is available free of charge on the ACS Publications website at DOI: 10.1021/acsbiomaterials.6b00585.

Tables S1–S3 and Figures S1–S9 (PDF)

■ AUTHOR INFORMATION

Corresponding Author

*E-mail: ebeniash@pitt.edu. Tel.: +1 412 6480108. Fax: +1 412 624 6685.

ORCID

Prashant N. Kumta: 0000-0003-1227-1249

Elia Beniash: 0000-0001-9019-5160

Notes

The authors declare no competing financial interest.

ACKNOWLEDGMENTS

The authors gratefully acknowledge the financial support of NSF-ERC, Grant EEC-0812348 (E.B., P.N.K.) and the Swanson School of Engineering Undergraduate Summer Research Program (O.J.). P.N.K. acknowledges the Edward R. Weidle in Chair Professorship Funds and the support of the Center for Complex Engineered Multifunctional Materials (CCEMM) in the Department of Bioengineering, Swanson School of Engineering, University of Pittsburgh, for providing funds towards acquisition of equipment to support the research. We thank John Holmes and Thorin Tobiassen from the Swanson Center for Product Innovation of the Swanson School of Engineering for aiding in the preparation of the samples, Jonathan Franks from the Center for Biological Imaging of at the University of Pittsburgh, Cole M. Van Ormer from the Department of Mechanical Engineering and Materials Science of the Swanson School of Engineering for providing their expertise in Scanning Electron Microscopy and Mr. Akhil Patel from the Department of Pharmaceutical Sciences, School of Pharmacy, University of Pittsburgh, for his help in confocal microscopy.

REFERENCES

- (1) Staiger, M. P.; Pietak, A. M.; Huadmai, J.; Dias, G. Magnesium and its alloys as orthopedic biomaterials: A review. *Biomaterials* **2006**, *27* (9), 1728–1734.
- (2) Witte, F.; Hort, N.; Vogt, C.; Cohen, S.; Kainer, K. U.; Willumeit, R.; Feyerabend, F. Degradable biomaterials based on magnesium corrosion. *Curr. Opin. Solid State Mater. Sci.* **2008**, *12* (5–6), 63–72.
- (3) Zhang, Y.; Xu, J.; Ruan, Y. C.; Yu, M. K.; O’Laughlin, M.; Wise, H.; Chen, D.; Tian, L.; Shi, D.; Wang, J.; Chen, S.; Feng, J. Q.; Chow, D. H. K.; Xie, X.; Zheng, L.; Huang, L.; Huang, S.; Leung, K.; Lu, N.; Zhao, L.; Li, H.; Zhao, D.; Guo, X.; Chan, K.; Witte, F.; Chan, H. C.; Zheng, Y.; Qin, L. Implant-derived magnesium induces local neuronal production of CGRP to improve bone-fracture healing in rats. *Nat. Med.* **2016**, *22*, 1160.
- (4) Chaya, A.; Yoshizawa, S.; Verdelis, K.; Myers, N.; Costello, B. J.; Chou, D. T.; Pal, S.; Maiti, S.; Kumta, P. N.; Sfeir, C. In vivo study of magnesium plate and screw degradation and bone fracture healing. *Acta Biomater.* **2015**, *18*, 262–269.
- (5) Yoshizawa, S.; Brown, A.; Barchowsky, A.; Sfeir, C. Magnesium ion stimulation of bone marrow stromal cells enhances osteogenic activity, simulating the effect of magnesium alloy degradation. *Acta Biomater.* **2014**, *10* (6), 2834–2842.
- (6) McBride, E. Absorbable metal in bone surgery: A further report on the use of magnesium alloys. *J. Am. Med. Assoc.* **1938**, *111* (27), 2464–2467.
- (7) Witte, F. The history of biodegradable magnesium implants: A review. *Acta Biomater.* **2010**, *6* (5), 1680–1692.
- (8) Hort, N.; Huang, Y.; Fechner, D.; Stormer, M.; Blawert, C.; Witte, F.; Vogt, C.; Drucker, H.; Willumeit, R.; Kainer, K. U.; Feyerabend, F. Magnesium alloys as implant materials - Principles of property design for Mg-RE alloys. *Acta Biomater.* **2010**, *6* (5), 1714–1725.
- (9) Cha, P. R.; Han, H. S.; Yang, G. F.; Kim, Y. C.; Hong, K. H.; Lee, S. C.; Jung, J. Y.; Ahn, J. P.; Kim, Y. Y.; Cho, S. Y.; Byun, J. Y.; Lee, K. S.; Yang, S. J.; Seok, H. K. Biodegradability engineering of microdegradable Mg alloys: Tailoring the electrochemical properties and microstructure of constituent phases. *Sci. Rep.* **2013**, *3*, DOI: [10.1038/srep02367](https://doi.org/10.1038/srep02367).
- (10) Hornberger, H.; Virtanen, S.; Boccaccini, A. R. Biomedical coatings on magnesium alloys - a review. *Acta Biomater.* **2012**, *8* (7), 2442–55.
- (11) Macdonald, M. L.; Samuel, R. E.; Shah, N. J.; Padera, R. F.; Beben, Y. M.; Hammond, P. T. Tissue integration of growth factor-eluting layer-by-layer polyelectrolyte multilayer coated implants. *Biomaterials* **2011**, *32* (5), 1446–1453.
- (12) Schmidmaier, G.; Wildemann, B.; Stemberger, A.; Haas, N. P.; Raschke, M. Biodegradable poly(D,L-lactide) coating of implants for continuous release of growth factors. *J. Biomed. Mater. Res.* **2001**, *58* (4), 449–455.
- (13) Reyes, C. D.; Petrie, T. A.; Burns, K. L.; Schwartz, Z.; Garcia, A. J. Biomolecular surface coating to enhance orthopaedic tissue healing and integration. *Biomaterials* **2007**, *28* (21), 3228–3235.
- (14) Nanci, A.; Wuest, J. D.; Peru, L.; Brunet, P.; Sharma, V.; Zalzal, S.; McKee, M. D. Chemical modification of titanium surfaces for covalent attachment of biological molecules. *J. Biomed. Mater. Res.* **1998**, *40* (2), 324–335.
- (15) Johnson, I.; Wang, S. M.; Silken, C.; Liu, H. N. A systemic study on key parameters affecting nanocomposite coatings on magnesium substrates. *Acta Biomater.* **2016**, *36*, 332–349.
- (16) Ostrowski, N.; Lee, B.; Enick, N.; Carlson, B.; Kunjukurju, S.; Roy, A.; Kumta, P. N. Corrosion protection and improved cytocompatibility of biodegradable polymeric layer-by-layer coatings on AZ31 magnesium alloys. *Acta Biomater.* **2013**, *9* (10), 8704–8713.
- (17) Doepke, A.; Xue, D.; Yun, Y.; Vanooij, W. J.; Brian Halsall, H.; Heineman, W. R. Corrosion of organosilane coated Mg4Y alloy in sodium chloride solution evaluated by impedance spectroscopy and pH changes. *Electrochim. Acta* **2012**, *70* (0), 165–170.
- (18) Witte, F.; Fischer, J.; Nellesen, J.; Vogt, C.; Vogt, J.; Donath, T.; Beckmann, F. In vivo corrosion and corrosion protection of magnesium alloy LAE442. *Acta Biomater.* **2010**, *6* (5), 1792–1799.
- (19) Cui, W.; Beniash, E.; Gawalt, E.; Xu, Z.; Sfeir, C. Biomimetic coating of magnesium alloy for enhanced corrosion resistance and calcium phosphate deposition. *Acta Biomater.* **2013**, *9* (10), 8650–8659.
- (20) Ehlert, N.; Mueller, P. P.; Stieve, M.; Behrens, P. Immobilization of alkaline phosphatase on modified silica coatings. *Microporous Mesoporous Mater.* **2010**, *131* (1–3), 51–57.
- (21) Liu, X.; Yue, Z.; Romeo, T.; Weber, J.; Scheuermann, T.; Moulton, S.; Wallace, G. Biofunctionalized anti-corrosive silane coatings for magnesium alloys. *Acta Biomater.* **2013**, *9* (0), 8671–8677.
- (22) Gaur, S.; Raman, R. K. S.; Khanna, A. S. In vitro investigation of biodegradable polymeric coating for corrosion resistance of Mg-6Zn-Ca alloy in simulated body fluid. *Mater. Sci. Eng., C* **2014**, *42*, 91–101.
- (23) Zheludkevich, M. L.; Salvado, I. M.; Ferreira, M. G. S. Sol-gel coatings for corrosion protection of metals. *J. Mater. Chem.* **2005**, *15* (48), 5099–5111.
- (24) Shimojima, A.; Kuroda, K. Structural Control of Multilayered Inorganic–Organic Hybrids Derived from Mixtures of Alkyltriethoxysilane and Tetraethoxysilane. *Langmuir* **2002**, *18* (4), 1144–1149.
- (25) Shimojima, A.; Kuroda, K. Designed synthesis of nanostructured siloxane–organic hybrids from amphiphilic silicon-based precursors. *Chem. Rec.* **2006**, *6* (2), 53–63.
- (26) Shimojima, A.; Sugahara, Y.; Kuroda, K. Synthesis of Oriented Inorganic–Organic Nanocomposite Films from Alkyltrialkoxysilane–Tetraalkoxysilane Mixtures. *J. Am. Chem. Soc.* **1998**, *120* (18), 4528–4529.
- (27) Chemtob, A.; Ni, L. L.; Croutxe-Barghorn, C.; Boury, B. Ordered Hybrids from Template-Free Organosilane Self-Assembly. *Chem. - Eur. J.* **2014**, *20* (7), 1790–1806.
- (28) de Araujo, A. D.; Palomo, J. M.; Cramer, J.; Kohn, M.; Schroder, H.; Wacker, R.; Niemeyer, C.; Alexandrov, K.; Waldmann, H. Diels-Alder ligation and surface immobilization of proteins. *Angew. Chem., Int. Ed.* **2006**, *45* (2), 296–301.
- (29) Adessi, C.; Matton, G.; Ayala, G.; Turcatti, G.; Mermod, J. J.; Mayer, P.; Kawashima, E. Solid phase DNA amplification: characterisation of primer attachment and amplification mechanisms. *Nucleic Acids Res.* **2000**, *28* (20), 87e.
- (30) Finnie, K. S.; Waller, D. J.; Perret, F. L.; Krause-Heuer, A. M.; Lin, H. Q.; Hanna, J. V.; Barbé, C. J. Biodegradability of sol–gel silica microparticles for drug delivery. *J. Sol-Gel Sci. Technol.* **2009**, *49* (1), 12–18.

- (31) Irimia-Vladu, M. "Green" electronics: biodegradable and biocompatible materials and devices for sustainable future. *Chem. Soc. Rev.* **2014**, *43* (2), 588–610.
- (32) Sanchez, C.; Julian, B.; Belleville, P.; Popall, M. Applications of hybrid organic-inorganic nanocomposites. *J. Mater. Chem.* **2005**, *15* (35–36), 3559–3592.
- (33) Sanchez, C.; Belleville, P.; Popall, M.; Nicole, L. Applications of advanced hybrid organic-inorganic nanomaterials: from laboratory to market. *Chem. Soc. Rev.* **2011**, *40* (2), 696–753.
- (34) Banerjee, P. C.; Raman, R. K. S. Electrochemical impedance spectroscopic investigation of the role of alkaline pre-treatment in corrosion resistance of a silane coating on magnesium alloy, ZE41. *Electrochim. Acta* **2011**, *56* (11), 3790–3798.
- (35) Witucki, G. L. A silane primer - chemistry and applications of alkoxy silanes. *J. Coat. Technol.* **1993**, *65* (822), 57–60.
- (36) Kokubo, T.; Takadama, H. How useful is SBF in predicting in vivo bone bioactivity? *Biomaterials* **2006**, *27* (15), 2907–2915.
- (37) Song, G.; Atrens, A.; StJohn, D.; Nairn, J.; Li, Y. The electrochemical corrosion of pure magnesium in 1 N NaCl. *Corros. Sci.* **1997**, *39* (5), 855–875.
- (38) Xin, Y.; Hu, T.; Chu, P. K. In vitro studies of biomedical magnesium alloys in a simulated physiological environment: A review. *Acta Biomater.* **2011**, *7* (4), 1452–1459.
- (39) Lorking, K. F. Inhibition of corrosion of magnesium in chromic acid. *Nature* **1964**, *201* (491), 75.
- (40) Bobe, K.; Willbold, E.; Morgenthal, I.; Andersen, O.; Studnitzky, T.; Nellesen, J.; Tillmann, W.; Vogt, C.; Vano, K.; Witte, F. In vitro and in vivo evaluation of biodegradable, open-porous scaffolds made of sintered magnesium W4 short fibres. *Acta Biomater.* **2013**, *9* (10), 8611–8623.
- (41) McCafferty, E. Validation of corrosion rates measured by the Tafel extrapolation method. *Corros. Sci.* **2005**, *47* (12), 3202–3215.
- (42) Shi, Z. M.; Liu, M.; Atrens, A. Measurement of the corrosion rate of magnesium alloys using Tafel extrapolation. *Corros. Sci.* **2010**, *52* (2), 579–588.
- (43) Kim, B. S.; Putnam, A. J.; Kulik, T. J.; Mooney, D. J. Optimizing seeding and culture methods to engineer smooth muscle tissue on biodegradable polymer matrices. *Biotechnol. Bioeng.* **1998**, *57* (1), 46–54.
- (44) Rampersad, S. N. Multiple Applications of Alamar Blue as an Indicator of Metabolic Function and Cellular Health in Cell Viability Bioassays. *Sensors* **2012**, *12* (9), 12347–12360.
- (45) Johnson, I.; Liu, H. In vitro Evaluation of Magnesium-based Metallic Biomaterials and the Need for Standardization. *Biomaterials Forum* **2012**, *34* (4), 9–14.
- (46) Bowen, P. K.; Drelich, J.; Goldman, J. Magnesium in the murine artery: Probing the products of corrosion. *Acta Biomater.* **2014**, *10* (3), 1475–1483.
- (47) Bowen, P. K.; McNamara, C. T.; Mills, O. P.; Drelich, J.; Goldman, J. FIB-TEM Study of Magnesium Corrosion Products after 14 Days in the Murine Artery. *ACS Biomater. Sci. Eng.* **2015**, *1* (10), 919–926.
- (48) Bowen, P. K.; Shearier, E. R.; Zhao, S.; Guillory, R. J.; Zhao, F.; Goldman, J.; Drelich, J. W. Biodegradable Metals for Cardiovascular Stents: from Clinical Concerns to Recent Zn-Alloys. *Adv. Healthcare Mater.* **2016**, *5* (10), 1121–1140.
- (49) Munemasa, J.; Kumakiri, T. Effect of the surface-roughness of substrates on the corrosion properties of films coated by physical vapor-deposition. *Surf. Coat. Technol.* **1991**, *49* (1–3), 496–499.
- (50) Grundmeier, G.; Schmidt, W.; Stratmann, M. Corrosion protection by organic coatings: electrochemical mechanism and novel methods of investigation. *Electrochim. Acta* **2000**, *45* (15–16), 2515–2533.
- (51) Stratmann, M.; Feser, R.; Leng, A. Corrosion protection by organic films. *Electrochim. Acta* **1994**, *39* (8–9), 1207–1214.
- (52) Ng, W. F.; Chiu, K. Y.; Cheng, F. T. Effect of pH on the in vitro corrosion rate of magnesium degradable implant material. *Mater. Sci. Eng., C* **2010**, *30* (6), 898–903.
- (53) Song, G.; Atrens, A.; StJohn, D. An Hydrogen Evolution Method for the Estimation of the Corrosion Rate of Magnesium Alloys. In *Magnesium Technology 2001*; John Wiley & Sons: 2001; pp 254–262.
- (54) Witte, F.; Fischer, J.; Nellesen, J.; Crostack, H.-A.; Kaese, V.; Pisch, A.; Beckmann, F.; Windhagen, H. In vitro and in vivo corrosion measurements of magnesium alloys. *Biomaterials* **2006**, *27* (7), 1013–1018.
- (55) Song, G. L.; Atrens, A. Understanding magnesium corrosion - A framework for improved alloy performance. *Adv. Eng. Mater.* **2003**, *5* (12), 837–858.
- (56) Duan, H. P.; Du, K. Q.; Yan, C. W.; Wang, F. H. Electrochemical corrosion behavior of composite coatings of sealed MAO film on magnesium alloy AZ91D. *Electrochim. Acta* **2006**, *51* (14), 2898–2908.
- (57) Stern, M.; Geary, A. L. Electrochemical Polarization: I. A Theoretical Analysis of the Shape of Polarization Curves. *J. Electrochem. Soc.* **1957**, *104* (1), 56–63.
- (58) Xin, Y. C.; Huo, K. F.; Tao, H.; Tang, G. Y.; Chu, P. K. Influence of aggressive ions on the degradation behavior of biomedical magnesium alloy in physiological environment. *Acta Biomater.* **2008**, *4* (6), 2008–2015.
- (59) Kramer, M.; Schilling, M.; Eifler, R.; Hering, B.; Reifenrath, J.; Besdo, S.; Windhagen, H.; Willbold, E.; Weizbauer, A. Corrosion behavior, biocompatibility and biomechanical stability of a prototype magnesium-based biodegradable intramedullary nailing system. *Mater. Sci. Eng., C* **2016**, *59*, 129–135.
- (60) Yang, L.; Zhang, E. L. Biocorrosion behavior of magnesium alloy in different simulated fluids for biomedical application. *Mater. Sci. Eng., C* **2009**, *29* (5), 1691–1696.
- (61) Cui, F.-z.; Yang, J.-x.; Jiao, Y.-p.; Yin, Q.-s.; Zhang, Y.; Lee, I.-S. Calcium phosphate coating on magnesium alloy for modification of degradation behavior. *Frontiers of Materials Science in China* **2008**, *2* (2), 143–148.
- (62) Gray-Munro, J. E.; Seguin, C.; Strong, M. Influence of surface modification on the in vitro corrosion rate of magnesium alloy AZ31. *J. Biomed. Mater. Res., Part A* **2009**, *91a* (1), 221–230.
- (63) Kunjukuju, S.; Roy, A.; Ramanathan, M.; Lee, B.; Candiello, J. E.; Kumta, P. N. A layer-by-layer approach to natural polymer-derived bioactive coatings on magnesium alloys. *Acta Biomater.* **2013**, *9* (10), 8690–703.
- (64) Park, M.; Lee, J. E.; Park, C. G.; Lee, S. H.; Seok, H. K.; Choy, Y. B. Polycaprolactone coating with varying thicknesses for controlled corrosion of magnesium. *Journal of Coatings Technology and Research* **2013**, *10* (5), 695–706.
- (65) Gupta, R. K.; Mensah-Darkwa, K.; Kumar, D. Corrosion Protective Conversion Coatings on Magnesium Disks Using a Hydrothermal Technique. *J. Mater. Sci. Technol.* **2014**, *30* (1), 47–53.
- (66) Zhu, Y. Y.; Wu, G. M.; Zhang, Y. H.; Zhao, Q. Growth and characterization of Mg(OH)(2) film on magnesium alloy AZ31. *Appl. Surf. Sci.* **2011**, *257* (14), 6129–6137.
- (67) Huo, H. W.; Li, Y.; Wang, F. H. Corrosion of AZ91D magnesium alloy with a chemical conversion coating and electroless nickel layer. *Corros. Sci.* **2004**, *46* (6), 1467–1477.
- (68) Ye, S.-H.; Jang, Y.-S.; Yun, Y.-H.; Shankaraman, V.; Woolley, J. R.; Hong, Y.; Gamble, L. J.; Ishihara, K.; Wagner, W. R. Surface Modification of a Biodegradable Magnesium Alloy with Phosphorylcholine (PC) and Sulfobetaine (SB) Functional Macromolecules for Reduced Thrombogenicity and Acute Corrosion Resistance. *Langmuir* **2013**, *29* (26), 8320–8327.
- (69) Lee, J. H.; Khang, G.; Lee, J. W.; Lee, H. B. Interaction of Different Types of Cells on Polymer Surfaces with Wettability Gradient. *J. Colloid Interface Sci.* **1998**, *205* (2), 323–330.
- (70) Ayala, R.; Zhang, C.; Yang, D.; Hwang, Y.; Aung, A.; Shroff, S. S.; Arce, F. T.; Lal, R.; Arya, G.; Varghese, S. Engineering the cell-material interface for controlling stem cell adhesion, migration, and differentiation. *Biomaterials* **2011**, *32* (15), 3700–3711.
- (71) Xu, L. P.; Pan, F.; Yu, G. N.; Yang, L.; Zhang, E. L.; Yang, K. In vitro and in vivo evaluation of the surface bioactivity of a calcium phosphate coated magnesium alloy. *Biomaterials* **2009**, *30* (8), 1512–1523.

(72) Curran, J. M.; Chen, R.; Hunt, J. A. Controlling the phenotype and function of mesenchymal stem cells in vitro by adhesion to silane-modified clean glass surfaces. *Biomaterials* **2005**, *26* (34), 7057–7067.

(73) Sauberlich, S.; Klee, D.; Richter, E. J.; Hocker, H.; Spiekermann, H. Cell culture tests for assessing the tolerance of soft tissue to variously modified titanium surfaces. *Clin. Oral Implants Res.* **1999**, *10* (5), 379–393.